RSC Advances

ROYAL SOCIETY OF CHEMISTRY

www.rsc.org/advances

Heteroepitaxial TiO_2@W-Doped VO_2 Core/Shell Nanocrystal Films: Preparation, Characterization, and Application as Bifunctional Window Coatings

Shi-Di Lan[1], Chi-Jung Chang[2], Chih-Feng Huang[3], Jem-Kun Chen[1]*

[1]Department of Materials Science and Engineering, National Taiwan University of Science and Technology, 43, Sec. 4, Keelung Rd, Taipei, 106, Taiwan, R.O.C.

[2]Department of Chemical Engineering, Feng Chia University, 100, Wenhwa Road, Seatwen, Taichung 40724, Taiwan, ROC

[3]Department of Chemical Engineering, National Chung Hsing University, Eng Bld 3,250 Kuo Kuang Road, 402 Taichung, Taiwan

*To whom correspondence should be addressed

E-MAIL: jkchen@mail.ntust.edu.tw

TEL.: 886-2-27376523

FAX: 886-2-27376544

Abstract

In this study we employed rutile TiO_2 nanoparticles (TiNPs) as cores for coating with vanadium sols of various concentrations and a tungsten doping of 2 at%. We grew the W-doped VO_2(M) nanocrystals (WVNCs) heteroepitaxially as shells onto the TiNP cores after a sintering process. Needle-like structures gradually appeared for the WVNCs on the TiNP surfaces upon increasing the concentration of the vanadium sol coating. These needle-like structures decreased the surface contact area sufficiently to result in superhydrophobicity. Falling water droplets rebounded completely from the TiNP@WVNC films, thereby potentially preventing fouling of such materials. The superhydrophobicity of a TiNP@WVNC film remained stable after 90 min of UV irradiation. The WVNC shells grew epitaxially on the TiNP seeds and enhanced the visible transmittance and near-infrared switching efficiency, due to the needle-like structures, similar to the behavior of an antireflection coating. In addition, the TiNP cores in the TiNP@WVNC films retained their photocatalytic properties completely. Such bifunctional (self-cleaning and thermochromic) nanomaterials might have applications in energy-saving smart windows.

Keywords: VO_2 nanocrystals; thermochromic; photocatalytic; superhydrophobic

1.Introduction

Increasingly sophisticated intelligent window coatings respond to an external stimulus in an "as needs" basis. Such materials include thermochromic coatings, which change their reflectance–transmission properties in response to temperature. Monoclinic-phase vanadium dioxide [VO_2(M)] is a promising material for use in thermochromic smart windows because its reversible insulator–metal phase transition (IMPT) between monoclinic and rutile phases [VO_2(M) ↔ VO_2(R)], at a phase transition temperature (T_p) of approximately 338 K, dramatically affects its electrical and optical properties.[1] VO_2(M) is a metallic material exhibiting high infrared reflection when the temperature is above T_p, but becomes a semiconductor with a reasonable infrared transmission when the temperature is below it.[2,3] The modulation of T_p to room temperature is essential for many practical applications, and not just limited to smart windows. A number of approaches have been reported for decreasing T_p; for example, doping of VO_2(M) with metal ions (e.g., W^{6+}, Mo^{6+}, Ta^{5+}, Nb^{5+}, Ru^{4+}) is a commonly used strategy, but it often decreases the thermochromic performance.[4]

Rutile TiO_2 has the same structure as VO_2(R) and quite similar lattice parameters. Because the crystal structure of VO_2 is sensitive to its under- and/or overcoating materials, rutile TiO_2 nanocrystals might be useful as seeds assisting the nucleation

and growth of nanostructured rutile VO_2. In the field of VO_2-based thermochromic smart windows, TiO_2 is also an important composite layer because of its good compatibility and crystalline structure similar to that of VO_2.[5] It has been reported that TiO_2 films are effective underneath layers or cover layers for inducing the crystallization of VO_2(M/R),[6] constructing heterostructures for photoemission,[7,8] enhancing the oxidation durability,[9,10] regulating the phase transition properties,[11] and improving the optical performance of VO_2.[1,12] Moreover, VO_2(M)/TiO_2 composites have their own attractions, not only for increasing visible transmittance but also for modifying the infrared modulation ability.[13,14] Relative to TiO_2–VO_2 multilayered structures, single-layered composite films are more attractive because of their ease of preparation, mixing homogeneity of the two components, and, most importantly, their display of near-infrared (NIR) modulation behavior at wavelengths significantly shorter than those for typical thin films of pure VO_2, thereby having advantages when applied in systems requiring efficient visible transmittance and NIR switching.[15]

Thin films of both TiO_2 and VO_2 can be prepared using a range of methods, primarily chemical vapor deposition (CVD),[16,17] sol–gel processing,[18,17] and physical vapor deposition (PVD).[20,21] CVD methods have the advantage of being more easily integrated into float-glass production lines. Although these methods can

provide single-layered TiO_2(A)–VO_2 through simultaneous deposition of TiO_2 and VO_2 at a critical temperature,[22,23] but the diffusion of Ti atoms into VO_2 crystal lattices weakens the thermochromic performance of VO_2.[24] The reported methods for fabricating VO_2(M)/TiO_2 composites are limited to using PVD, which cannot meet the requirements for the production of large-area VO_2 thermochromic windows because of technical and cost problems. Because the crystallization temperature of TiO_2(A) is much lower than that of VO_2(R),[25] a "two-step method" method has been developed for producing TiO_2(A)/VO_2 single-layered composite films, in which VO_2 nanoparticles (NPs) are first prepared and dispersed in a titanium sol to form a composite film and then annealed for TiO_2 crystallization. This method largely restricts Ti diffusion and maintains the thermochromic performance of VO_2. As such, the resulting materials become more cost-effective for large-scale coatings of glass. It has been demonstrated recently that combining TiO_2 and VO_2 within a phase composite produces a material that possesses both self-cleaning and thermochromic properties.[26,27] Furthermore, the films exhibited a 17 °C decrease in the thermochromic switching temperature (T_p) to 51 °C. If this value of T_p could be lowered further, such coatings would be strong candidates for application in self-cleaning solar control glazing. In this paper, we report a "two-step method" for the preparation of TiO_2/VO_2 composites in which rutile TiO_2 nanoparticles (TiNPs)

are first dispersed in a W-doped vanadium sol to form a composite film that is then annealed to ensure crystallization of the W-doped VO_2. We have found that the specific needle-like structures of the W-doped VO_2 nanocrystals (WVNCs) could be regulated by varying the ratio of TiO_2 cores to VO_2 shells. Films of the as-prepared composite particles on glass exhibited remarkable superhydrophobicity and hysteresis widths considerably narrower than that of pure VO_2. Furthermore, this specific morphology increased the visible transmittance of the film and enhanced its regulation ability. Such films performed triple functions: thermochromism (from the VO_2(M) layer) for solar energy modulation, photocatalysis (of the TiNPs), and superhydrophobicity (for antifouling and self-cleaning effects). The as-obtained nanocomposite coatings appear to have applicability in smart windows.

2.Experimental Section

2.1 Materials

Vanadium pentoxide (V_2O_5, Acros Organics, >99.6%) and tungsten(VI) oxide (WO_3, Hayashi Pure Chemical Industries, >99%) were employed as starting materials to prepare VO_2^+ solutions. Rutile TiNPs (sizes: 11–20 nm; Acros Organics; CAS No. 13463-67-7) were used as received. Methylene Blue ($C_{16}H_{18}ClN_3S$, MB, 98%) was purchased from Aldrich. All other chemicals and solvents were of reagent grade and purchased from Aldrich. All reagents were used without further purification.

2.2 TiNPs@WVNCs Films

TiNPs (ca. 0.02–0.05 g) were dispersed ultrasonically in anhydrous EtOH (50 mL) for 15 min. An aqueous solution of the surfactant Triton X-100 (Sigma Aldrich, 800 μL, 0.1 M) was added into the suspension, which was then stirred for 2 h. Another stock aqueous sol was produced using a method previously reported[28]: heating V_2O_5 powder (15 g) in a crucible until molten and then pouring it into distilled water at room temperature. After vigorous stirring, the sol was filtered, thus establishing solutions of various concentrations (ca. 1, 2, 3, and 4 at. %). Tungsten(VI) oxide powder was dissolved in a few drops of distilled water and added to the sol, in quantities calculated to achieve a doping level (assuming 100% substitution) of 2 at. %. The stock solution was subsequently added dropwise into the TiNP suspension, followed by sonication for 30 min prior to use. Soda lime glass slides were cleaned ultrasonically for 10 min in 20% EtOH, 20% acetone, and deionized water. After drying the glass slides by purging with N_2, they were subjected to argon/oxygen plasma (AOP) treatment using a TCP 9400SE instrument (Lam Research).[29] AOP treatment caused the surface to become chemically modified (strongly hydrophilic or polar). The introduction of these polar groups provided a more polar surface for formation of the film. For each coating the sol was spin-coated on the AOP-treated glass slides, then dried in a clean air cabinet for 10–15 min. The TiNP@WVNC films

on the AOP-treated glass substrates were obtained after spin-coating at a speed of 3000 rpm. To obtain a crystalline coating, the as-obtained films were sintered in a vacuum quartz tube furnace under a low pressure of a reducing gas mixture (50% CO, 50% CO_2). Typically at a pressure of approximately 3 torr, the sample was heated from ambient temperature to 500 ℃ at a heating rate of approximately 20 °C/min and then held at 500 ℃ for 2 h before being naturally cooled to room temperature. The annealing program was optimized to transform the amorphous shells into crystallized VO_2(M) while keeping the TiO_2 cores chemically intact. The samples of TiNPs that had been coated with the 1, 2, 3, and 4 at. % vanadium sols and then sintered are denoted herein as TV1, TV2, TV3, and TV4, respectively.

2.3 Characterization of Heteroepitaxial TiNPs@WVNCs Films

The valence states of vanadium, tungsten, and titanium were studied using X-ray photoelectron spectroscopy (XPS; Scientific Theta Probe, UK). The structures of the samples were determined through X-ray diffraction (XRD; Rigaku D/max-RC). The phase transition behavior was analyzed through differential scanning calorimetry (DSC; Netzsch DSC-4000) at a temperature ramp rate of 10 °C/min within the –20 to +100 °C range under a flowing N_2 atmosphere. The chemical compositions of the as-obtained samples were revealed using energy-dispersive X-ray spectrometry (EDX) combined with high-resolution scanning electron microscopy (HR-SEM; JEOL

JSM-6500F, Japan). Transmission electron microscopy (TEM) images were obtained using a field emission transmission electron microscope (Philips Tecnai G2 F20) operated at an accelerating voltage of 200 kV. Static water contact angles (SWCAs) were measured using a FDSA MagicDroplet-100 contact angle goniometer. Each SWCA was determined, under normal laboratory ambient conditions at room temperature under 40% of humidity, by fitting a Young–Laplace curve around the drop. Each mean value was calculated from at least 10 individual measurements; the measurement error was less than 3°. As-prepared superhydrophobic surfaces were mounted on a rotatable stage. The stage was tilted until a droplet on the stage slid, thereby characterizing the roll-off angle of the surface. The tilt angle of the surface was fixed at a certain angle. The changes in the SWCAs after UV irradiation were monitored at specific time intervals.

2.4 TiNP@WVNC Films for Applications in Bifunctional Smart Windows

The TiNP@WVNC films underwent a reversible IMPT, which was accompanied by remarkable changes in their optical properties. Optical transmittances were monitored using a UV−vis−near-infrared spectrophotometer (Shimadzu UV3600) equipped with a thermo-regulated environmental cell. The reversible IMPT temperatures of the thin films were measured by recording the transmittance spectra as a function of temperature. For all samples, the integral visible transmittance (T_{int}) was obtained

based on the measured spectra using the following equation:[30]

$$X_\rho = \frac{\int \phi_\rho(\lambda) X(\lambda) d\lambda}{\int \phi_\rho(\lambda) d\lambda} \qquad (1)$$

where X denotes the transmittance measured through UV−vis−near-infrared spectrophotometer. The values of T_{int} were obtained using the formula $\phi_\rho = \Phi_{lum}$, where Φ_{lum} was the standard luminous efficiency function and $\Phi_{lum} = 0$ beyond this range.

The photocatalytic performance of the synthesized TiNP@WVNC films was determined by evaluating the rate of degradation of MB. A glass plate (1 × 1 cm) presenting a thin TiNP@WVNC film was immersed in aqueous MB solution (20 ppm, 20 mL). The sample was kept in the dark to allow complete absorption of MB onto the surface; it was then irradiated using a UV lamp. The concentration of MB in the solution was measured as a function of the irradiation time, monitoring the wavelength of maximum absorbance (λ_{max}) of MB at 664 nm. Photometric analysis of the TiNP@WVNC films before and after irradiation was performed to measure the degradation efficiency of MB (D%), defined using the expression [11]

$$D\% = 100 \times \frac{C_0 - C}{C_0} \qquad (2)$$

where C_0 is the initial concentration of MB and C is the concentration of MB after irradiation of the samples for a period of time. The absorbances of the samples were measured using a UV–Vis spectrophotometer having a resolution of 1 nm

(Perkin–Elmer, lambda 25, 190–1100 nm). The decrease in the absorbance at λ_{max} of the samples after irradiation for a desired period of time allowed determination of the rate of decolorization and, therefore, the MB photodegradation efficiency, which also represented the activity of the TiNP@WVNC films. The following equation was used to measure the rate of MB degradation (k) at a given time:

$$\ln\frac{C_0}{C} = kt \qquad (3)$$

For comparison, thin films of a commercially available pure TiO_2 catalyst were also examined under similar conditions.

3. Results and Discussion

3.1 Characterization and Heteroepitaxy of TiNP@WVNC Films

The synthesis of the TiNP@WVNC films in this study can be regarded as a process of generating "TiNP seeds" upon which the VO_2 crystals grew. We used sol–gel deposition to produce uniform precursor shells of various thicknesses on the TiO_2 cores. We used XPS to investigate the chemical states on the surfaces of the as-obtained TiNP@WVNC films; Figure 1a indicates that the sample consisted of only six elements: carbon, vanadium, titanium, oxygen, silicon, and tungsten. The presence of signals for carbon and silicon atoms presumably reflected surface contamination and the glass slides, respectively. For the vanadium precursor film, we assign the peaks centered at 517.15 and 524.2 eV to the V 2p3/2 and V 2p1/2 orbitals,

respectively. The signal for the V 2p3/2 orbitals of the sample appeared at a binding energy of 517.8 eV, attributable to V^{5+}.[31]. In addition, two peaks were centered at 529.6 and 532.2 eV in the O 1s region (Figure 1b). We assign the major peak, positioned at the lower binding energy of 529.6 eV, to the O^{2-} ions in V–O bonding [32]. We assign the second peak, located at 532.2 eV, to OH^- groups in H_2O molecules. The XPS V 2p core-level spectrum recorded after sintering of the sample revealed (Figure 1c) that the V 2p doublet binding energies were 516.85 and 524.32 eV, corresponding to spin-orbits splitting of the V 2p3/2 and V 2p1/2 components, respectively [33]. The V 2p3/2 peak could be split into major and minor peaks at 516.85 and 515.7 eV. The major V 2p3/2 peak shifted from 517.15 to 516.85 eV after sintering, suggesting the generation of V^{4+} species. The V 2p3/2 binding energy was slightly higher than that of pure VO_2, but was in agreement with the value (516.3 eV) for W-doped VO_2 [34], suggesting that the V 2p3/2 binding energy increased slightly after W-doping and that the vanadium atoms in the doped sample resided in the +4 oxidation state. The minor V 2p3/2 peak at 515.7 eV could be assigned to V-Ti bonding.[35] We attribute the binding energies at 458.15 and 464.25 eV to the Ti 2p3/2 and Ti 2p1/2 binding energies, respectively, of the rutile-phase TiNP (Figure 1d), corresponding to the position for Ti^{4+} species in TiNP (the reported value for pure Ti is 458.0–458.5 eV [25]). Figure 1e displays signals for the W 4f species in the sample,

with W 4f5/2 and W4f7/2 binding energies centered at 37.7 and 35.7 eV, respectively. According to the standard binding energies, there was only a small amount of tungsten in the sample, with the oxidation state of the tungsten ions in these films being solely W^{6+}. Table 1 lists the ratios of titanium to vanadium (Ti/V) in the samples TV1, TV2, TV3, and TV4. We observe that the Ti/V ratio decreased upon increasing the concentration of the vanadium sol coating on the TiNPs.

Figure 2 displays XRD patterns of the WVNC powders TV1, TV2, and TV4 and of pure TiNP. The observed diffraction peaks of the pure WVNC powders can be indexed to the monoclinic phase of VO_2(M) (JCPDS card no. 43-1051). No noticeable changes in the positions of the diffraction peaks occurred for samples TV1, TV2, and TV4, but they had shifted to a slightly lower angle when compared with that the sample prepared without the TiO_2 cores; this shift could have resulted from superposition of the diffraction peaks from rutile TiO_2 and VO_2(M), both near 27.8°. For TV1, TV2, and TV4, we observed XRD peaks for both VO_2(M) and rutile TiO_2. The intensity of the VO_2(M) peak increased upon increasing the thickness of the coating on the TiNPs, consistent with the formation of VO_2(M) shells.

Endothermic and exothermic peaks were evident in each DSC curve (Figure 3), further confirming the formation of VO_2(M). Table 1 lists the values of T_p in the heating cycle and hysteresis (ΔT_H) between the heating and cooling cycle, recorded

from the DSC curves, for TV1, TV2, TV3, and TV4. The value of T_p increased upon increasing the TiNP seed content despite having the same W doping content (e.g., T_p increased from 29.8 to 34.1 °C when the Ti/V molar ratio increased from 0.25 to 1.61). This result suggests that addition of the TiNP seeds suppressed the W doping content in VO_2(M). The latent heats calculated from the heating cycles in Figure 3 were 38.5 and 15.7 J/g for the WVNCs prepared with and without TiNP seeds. The higher latent heat indicates that the TiNP@WVNCs were highly crystalline and relatively perfect in their crystalline structure.[36] The hysteresis between the heating and cooling cycles increased upon increasing the content of TiO_2 seeds (from 2.7 to 5.6 °C), in contrast to the reported result that TiO_2 additives can remarkably narrow the hysteresis loop width;[37] we suspect that it is due to the effect of the morphology of the TiNP@WVNCs.[38]

We used SEM to characterize the surface morphologies and nanostructures of our samples. Figure 4 displays SEM images and EDX analyses of the TiNPs coated using the 1, 2, 3, and 4 at. % vanadium sols. The vanadium sols generated homogeneous thin films on the TiNPs prior to sintering, resulting in similar morphologies for the four samples (Figures 4a–d). The thicker shells tended to assemble through neck-connecting because of the lower number of heterogeneous nucleation sites.[39] Crystalline structures appeared for the films after sintering, due to formation of VO_2

nanocrystals. Needle-like structures appeared initially on the TiNP surfaces of TV1 (Figure 5a); their lengths ranged from 100 to 500 nm, indicating irregular thicknesses of the vanadium sol coating. For TV2, the needle-like structures of the WVNCs covered the entire surfaces of the TiNPs with more regular lengths ranging from 70 to 150 nm (Figure 5b). Further increasing the concentration of the precursor sol to 3 at.% caused the needle-like structures to exhibit high regularity (lengths: ca. 300 nm) on the surfaces of the TiNPs (Figure 5c). An urchin-like structure appeared for the WVNCs of TV4, indicating that aggregation of the TiNP cores had occurred at a 4 at. % vanadium sol coating on the TiNPs (Figure 5d). In the absence of the TiO_2 seeds, the VO_2(M) had an irregular shape.[40] The roughnesses, measured using AFM, in Table 1 confirm that the WVNC coatings had significantly different morphologies and Ti/V ratios in the samples TV1, TV2, TV3, and TV4. After annealing, the core/shell interface became obscure (Figure 6a), indicating that the shell coating crystallized with a relatively rough morphology. The needle-like structures of the WVNCs on the surfaces of the TiNPs were clearly evident for TV3. The lattice-resolved HRTEM images of TV3 revealed distinguishable crystallographic lattice fringes, with the lattices coherently bound to the TiO_2 side faces (Figure 6b). We could distinguish two different lattices for VO_2 and TiO_2, with nearly orthogonal and oblique crossing patterns (represented schematically in the rectangular region), respectively. The

interplanar distances of 0.332 nm in the yellow region and 0.324 nm in the green match well with the (-111) and (110) crystal planes of VO_2(M) and rutile TO_2, respectively, suggesting that the VO_2(M) crystals grew epitaxially on the rutile TiNPs; the appearance of a dislocation in the interface region, arising from the slightly different interplanar distances in VO_2(M) and rutile TiNP, confirmed this epitaxial growth. Thus, a coupled interface existed between the VO_2 and TiO_2 phases, with the surfaces of the TiO_2 cores serving as propitious sites for heterogeneous nucleation of the VO_2 phase. We performed EDS analysis of the shell coating, applying a beam spot size of less than 1 nm. Signals we detected for both V and Ti coexisting in the shell, indicating some degree of Ti–V diffusion at the core/shell interface, presumably because of the infinite solubility of Ti in VO_2 lattices.[35] This finding also suggests that rutile TiO_2 seeds can induce the epitaxial growth of VO_2(M) nanocrystals.

When a liquid droplet is placed in contact with a superhydrophobic surface capable of self-cleaning, a high contact angle is formed with a small interfacial area between the liquid and the surface. In the ideal situation, the liquid would not wet the surface and would be free to roll off from it. This surface property, caused by the surface energy of the solid being lower than that of the liquid, results from either the chemistry of the material or its physical roughness, including both nanometer- and micrometer-scale features. Figure 7a presents the SWCAs and roll-off angles of the

surfaces of pure TiNPs, TV1, TV2, TV3, and TV4. Water droplets on the pure TiO_2 surface and TV1, TV2, TV3, and TV4 surfaces provided SWCAs of 85 ± 3, 139 ± 3, 151 ± 3, 163 ± 3, and 155 ± 3°, respectively. Thus, the SWCAs of the heteroepitaxial surfaces were larger than that of the pure-TiNP surface. The SWCAs of the surfaces increased gradually upon increasing the fraction of needle-like WVNC structures up to that in TV3, but did not change significantly thereafter. Prior to UV irradiation, the water droplets on the pure TiNP and TV1 and TV2 surfaces exhibited roll-off angles of 47 ± 3, 18 ± 3, and 11 ± 3°, respectively; increasing the density of needle-like structures even further, to give the TV3 and TV4 surfaces, caused the roll-off angles to decrease abruptly to approximately 1 ± 3°. The water droplets penetrated the TV1 and TV2 surfaces because of their lower densities of needle-like WVNC structures, resulting in relatively large roll-off angles. When water droplets resided on the TV3 and TV4 surfaces, with their greater fractional coverages of needle-like structures, air was presumably trapped in the cavities of these rough surfaces, resulting in composite solid–air–liquid interfaces and, therefore, relatively low roll-off angles. Figures 7b and 7c display the SWCAs and roll-off angles, respectively, of the pure TiNP surface and the TV1, TV2, TV3, and TV4 surfaces, plotted with respect to the UV irradiation time. VO_2(M) is a well-known semiconductor material with a band gap of 0.7 eV, and is seldom used as a photocatalyst. UV irradiation may not always change the VO_2(M)

and VO_2(M) is not always oxidized under UV irradiation. The SWCA of pure TiNP surface was affected significantly, forming a completely hydrophilic surface (SWCA: <5°), upon increasing the UV irradiation time to 100 min (Figure 7b). The SWCAs of the TV1 and TV2 surfaces decreased gradually, to 113 and 133°, respectively, within 180 min because of their lower densities of needle-like structures. The SWCAs of TV3 and TV4 did not change significantly within 180 min of UV irradiation, due to their lower surface ratios—the fraction of the surface area over the total geometric area of a sample, an indicator of the grooving of the surface that allows air pockets to form between the solid surface and the overlaying liquid droplet. Figure 7c plots the roll-off angles with respect to the UV irradiation time for the pure TiNP surface and the TV1, TV2, TV3, and TV4 surfaces; data points marked with a roll-off angle of 90° represent droplets that were pinned to the substrates even when tilted vertically or flipped upside down. As expected, the roll-off angles for the pure TiNP surface and the TV1 and TV2 substrates increased upon increasing the UV irradiation time, eventually reaching a state where the water droplet remained stuck to the surface even when it was turned by 90°. The roll-off angles of TV3 and TV4 did not change significantly within 180 min of UV irradiation. Such highly stable superhydrophobicity after UV irradiation may extend the lifetimes of smart windows. Impact experiments revealed that the needle-like structures exhibited superior

slippage and robustness of their superhydrophobicity. We allowed water droplets to fall onto 35°-tilted pure TiNP and TV3 surfaces to observe their stickiness and rebound ability, respectively. We released droplets of 1-mm radius from rest at a height of 4.5 mm. In Figures 7d and 7e, the substrates were tilted at an angle of 35° to monitor their rebound trajectories. For the pure TiNP surface, the droplets stuck to the surface (Figure 7d). When needle-like WVNC structures were present on the TV3 surface, the droplets bounced completely from the substrate (Figure 7e). Thus, needle-like structures improved the slippage of droplets on pure TiNP surfaces, resulting in effective rebounding.

3.2 TiNP@WVNC Films for Applications in Bifunctional Smart Windows

The values of T_{int} and the NIR switching efficiency (E_s) are the two main parameters characterizing smart windows. Although these two parameters are strongly related, their changes can be conflicting.[41] A large visible transmittance is usually accompanied by a small value of E_s, and vice versa. Developing methods to improve the value of E_s while simultaneously maintaining a comparatively high visible transmittance has been challenging. We studied the thermochromic properties of the TiNP@WVNC films by measuring the optical transmittance spectra of TV1, TV2, TV3, and TV4. Figure 8a reveals that all of these films displayed excellent visible transmittance at 20 and 50 °C as well as excellent values of E_s. For the TV1, TV2,

TV3 and TV4 films that were coated at a thickness of approximately 87 nm, the values of T_{int} of the semiconductive states reached 31, 44, 62, and 64%, respectively, with values of E_s in the range 20–45% (Table 1). The values of T_{int} for TV3 and TV4 are higher than those for single-layer VO_2 coatings of similar film thicknesses (reported values for 50-nm-thick films include 40 and 45%).[42] Thus, the needle-like structured surfaces can be regarded as antireflecting coatings (ARCs) with enhanced transmittance.[43] It is rare for single-layer VO_2 crystals to display optical performance that includes high values of T_{int} and good values of E_s; thus, our current solution-based method appears to have many advantages over other preparation methods.

To test the applicability of the photocatalytic effects to smart windows, we immersed our TiNP@WVNC films into a reaction solution containing MB for various lengths of time. Figure 8b displays the absorption of a solution of MB after UV irradiation in the presence of the TV3 film (0 min: time at which the container was placed in the dark). The TiNP cores coated with the WVNC shells retained their photocatalytic properties, exciting electron/hole pairs under UV light. The rate of MB degradation (k) over thin films of commercial TiNPs (particle size: 20 nm; P25) was approximately 0.0013. Apart from TV1, the rates of MB degradation over the thin films of TiNP@WVNC were all higher than that of over the commercial TiNPs (Table

1). We suspect that the heteroepitaxial crystallinity induced the photocatalytic ability of VO_2 and, thereby, enhanced the rate of MB degradation. Therefore, these heteroepitaxial TiNP@WVNC systems exhibited bifunctional properties—superior thermochromicity and photoactivity—under UV radiation, due to their large surface areas, relative to those of thin films of pure TiNPs.

4.Conclusion

TiNPs can be coated heteroepitaxially with WVNCs, resulting in needle-like structured nanocrystals on the surfaces. The morphology changed from the particle shape of rutile TiNP in the absence of the vanadium sol coating to needle-like shapes for the TiNP@WVNCs. Films of the needlelike-structured TiNP@WVNCs exhibit superhydrophobicity (SWCA: >150°) and could rebound water droplets completely. The needle-like structures of the heteroepitaxial nanocrystals enhanced the modulation of the visible transmittance substantially. In addition, the TiNP cores within the W-doped VO_2 shells retained their photocatalytic properties completely. This study not only provides a simple means for synthesizing core/shell TiNP@WVNC films for dual-functional (photocatalytic and thermochromic) window coatings but also demonstrates their stable superhydrophobicity after UV irradiation.

Acknowledgment

We thank the Ministry of Science and Technology of the Republic of China for supporting this research financially.

References

[1] Park, J. H.; Coy, J. M.; Kasirga, S.; Huang, C.; Fei, Z.; Hunter, S.; Cobden, D. H. Measurement of a solid-state triple point at the metal–insulator transition in VO_2. *Nature* 2013, 500, 431–434.

[2] Case, F. C. Improved VO_2 thin films for infrared switching. *Appl. Opt.* 1991, 30, 4119–4123.

[3] Beteille, F.; Livage, J. Optical switching in VO_2 thin films. *J. Sol–Gel Sci. Technol*. 1998, 13, 915–921.

[4] Goodenough, J. B. The two components of the crystallographic transition in VO_2. *J. Solid State Chem.* 1971, 3, 490–500.

[5] Hervieu, M. The surface science of metal oxides. *Adv. Mater.* 1995, 7, 91–92.

[6] Muraoka Y.; Hiroi, Z. Metal–insulator transition of VO_2 thin films grown on TiO_2 (001) and (110) substrates. *Appl. Phys. Lett.* 2002, 80, 583–585.

[7] Okazaki, K.; Wadati, H.; Fujimori, A.; Onoda, M.; Muraoka, Y.; Hiroi, Z. Photoemission study of the metal–insulator transition in VO_2/TiO_2 (001): Evidence for strong electron–electron and electron–phonon interaction. *Phys. Rev. B: Condens. Matter Mater. Phys.* 2004, 69, 165104.

[8] Eguchi, R.; Shin, S.; Fukushima, A.; Kiss, T.; Shimojima, T.; Muraoka, Y.; Hiroi, Z. Thermoelectric properties and figure of merit of a Te-doped InSb bulk single crystal. *Appl. Phys. Lett.* 2005, 87, 201902.

[9] Zhang, Z. T.; Gao, Y. F.; Kang, L. T.; Du, J.; Luo, H. J. Effects of a TiO_2 buffer layer on solution-deposited VO_2 films: Enhanced oxidization durability. *J. Phys. Chem. C* 2010, 114, 22214–22220.

[10] Fu, G.; Polity, A.; Volbers, N.; Meyer, B. K. Annealing effects on VO_2 thin films deposited by reactive sputtering. *Thin Solid Films* 2006, 515, 2519–2522.

[11] Chen, J.; He Y.; Li, C. Synthesis of doubly functional nanowhiskers from a colloid solution including a V–Ti complex precursor. *J. Mater. Sci*. 2012, 47, 5287–5297.

[12] Kang, L.; Gao, Y.; Luo, H.; Chen, Z.; Du, J.; Zhang, Z. Nanoporous thermochromic VO(2) films with low optical constants, enhanced luminous transmittance and thermochromic properties. *ACS Appl Mater Interfaces* 2011, 3, 135–138.

[13] Wilkinson, M.; Kafizas, A.; Bawaked, S. M.; Obaid, A. Y.; Al-Thaiti, S. A.; Basahel, S. N.; Carmalt, C. J.; Parkin, I. P. Combinatorial atmospheric pressure chemical vapor deposition of graded TiO_2–VO_2 mixed-phase composites and their

dual functional property as self-cleaning and photochromic window coating. *ACS Comb. Sci.* 2013, 15, 309–319.

[14] Mlyuka, N. R.; Niklasson, G. A.; Granqvist, C. G. Thermochromic multilayer films of VO_2 and TiO_2 with enhanced transmittance. *Sol. Energy Mater. Sol. Cells* 2009, 93, 1685–1687.

[15] Li, S. Y.; Niklasson, G. A.; Granqvist, C. G. Nanothermochromics: Calculations for VO_2 nanoparticles in dielectric hosts show much improved luminous transmittance and solar energy transmittance modulation. *J. Appl. Phys.* 2010, 108, 063525.

[16] Manning, T. D.; Parkin, I. P.; Blackman, C. S.; Qureshi, U. APCVD of thermochromic vanadium dioxide thin films–solid solutions $V_{2-x}M_xO_2$ (M = Mo, Nb) or composites VO_2–SnO_2. *J. Mater. Chem.* 2005, 15, 4560–4566.

[17] O'Neill, S. A.; Clark, R. J. H.; Parkin, I. P.; Elliott, N.; Mills, A. Anatase thin films on glass from the chemical vapor deposition of titanium(IV) chloride and ethyl acetate. *Chem. Mater.* 2003, 15, 46–50.

[18] Kafizas, A.; Dunnill, C. W.; Parkin, I. P. The relationship between photocatalytic activity and photochromic state of nanoparticulate silver surface loaded titanium dioxide thin-films. *Phys. Chem. Chem. Phys.* 2011, 13, 13827–13838.

[19] Partlow, D. P.; Gurkovich, S. R.; Radford, K. C.; Denes, L. J. Switchable vanadium oxide films by a sol–gel process. *J. Appl. Phys.* 1991, 70, 443.

[20] Martin, N.; Rousselot, C.; Rondot, D.; Palmino, F.; Mercier, R. Microstructure modification of amorphous titanium oxide thin films during annealing treatment. *Thin Solid Films* 1997, 300, 113–121.

[21] Lee, M.-H.; Kim, M.-G. RTA and stoichiometry effect on the thermochromism of VO2 thin films. *Thin Solid Films* 1996, 286, 219–222.

[22] Kakiuchida, H.; Jin, P.; Tazawa, M. Optical characterization of vanadium titanium oxide films. *Thin Solid Films* 2008, 516, 4563–4567.

[23] Du, J.; Gao, Y. F.; Luo, H. J.; Kang, L. T.; Zhang, Z. T.; Chen, Z.; Cao, C. X. Significant changes in phase-transition hysteresis for Ti-doped VO_2 films prepared by polymer-assisted deposition. *Sol. Energy Mater. Sol. Cells* 2011, 95, 469–475.

[24] Balberg, I.; Abeles, B.; Arie, Y. Phase transition in reactively co-sputtered films of VO_2 and TiO_2. *Thin Solid Films* 1974, 24, 307–310.

[25] Li, R.; Ji, S. D.; Li, Y. M.; Gao, Y. F.; Luo, H. J.; Jin, P. Synthesis and characterization of plate-like VO_2(M)@SiO_2 nanoparticles and their application to smart window. *Mater. Lett.* 2013, 110, 241–244.

[26] Qureshi, U.; Manning, T. D.; Blackman, C.; Parkin, I. P. Composite thermochromic thin films: (TiO_2)–(VO_2) prepared from titanium isopropoxide, $VOCl_3$ and water. *Polyhedron* 2006, 25, 334–338.

[27] Qureshi, U.; Manning, T. D.; Parkin, I. P. Atmospheric pressure chemical vapour deposition of VO_2 and VO_2/TiO_2 films from the reaction of $VOCl_3$, $TiCl_4$ and water. *J. Mater. Chem.* 2004, 14, 1190–1194.

[28] Hanlon, T. J.; Coath, J.A.; Richardson, M.A. Molybdenum-doped vanadium dioxide coatings on glass produced by the aqueous sol–gel method. *Thin Solid Films* 2003, 436, 269–272.

[29] Chen, J. K.; Hsieh, C. Y.; Huang, C. F.; Li, P. M.; Kuo, S. W.; Chang, F. C. *Macromolecules* 2008, 41, 8729–8736.

[30] Cao, C. X.; Gao Y. F.; Luo, H. J. Pure single-crystal rutile vanadium dioxide powders: Synthesis, mechanism and phase-transformation property. *J. Phys. Chem. C* 2008, 112, 18810–18814.

[31] Wang, Y.; Zhang, Z. Synthesis and transport properties of nanostructured VO_2 by mechanochemical processing. *Phys. E* 2009, 41, 548–551.

[32] Cui, C. J.; Wu, G. M.; Shen, J.; Zhou, B.; Zhang, Z. H.; Yang, H. Y.; She, S. F. Synthesis and electrochemical performance of lithium vanadium oxide nanotubes as cathodes for rechargeable lithium-ion batteries. *Electrochim. Acta* 2010, 55, 2536–2541.

[33] Zhang, Y.; Liu, X.; Xie, G.; Yu, L.; Yi, S.; Hu, M.; Huang, C. Hydrothermal synthesis, characterization, formation mechanism and electrochemical property of $V_3O_7 \cdot H_2O$ single-crystal nanobelts. *Mater. Sci. Eng. B* 2010, 175, 164–171.

[34] Li, F.; Wang, X. H.; Shao, C. L.; Tan R. X.; Liu, Y. C. Biodegradable polyester hybrid nanocomposites containing titanium dioxide network and poly(ε-caprolactone): Synthesis and characterization. *Mater. Lett.* 2007, 61, 1328–1332.

[35] Li, Y.; Ji, S.; Gao, Y.; Luo, H.; Jin, P. Modification of Mott phase transition characteristics in VO_2@TiO_2 core/shell nanostructures by misfit-strained heteroepitaxy. *ACS Appl. Mater. Interfaces* 2013, 5, 6603–6614.

[36] Chen, Z.; Gao, Y. F.; Kang, L. T.; Cao, C. X.; Chen, S.; Luo, H. Fine crystalline VO_2 nanoparticles: Synthesis, abnormal phase transition temperatures and excellent optical properties of a derived VO_2 nanocomposite foil. *J. Mater. Chem. A* 2014, 2, 2718–2727.

[37] Li, Y.; Ji, S.; Gao, Y.; Luo, H.; Kanehira, M. Core–shell VO_2@TiO_2 nanorods that combine thermochromic and photocatalytic properties for application as energy-saving smart coatings. *Sci. Rep*. 2013, 3, 1370–1373.

[38] Suh, J. Y.; Lopez, R.; Feldman, L. C.; Haglund, R. F. Semiconductor to metal phase transition in the nucleation and growth of VO_2 nanoparticles and thin films. *J. Appl. Phys.* 2004, 96,1209–1212.

[39] Demirörs, A. F.; van Blaaderen, A.; Imhof, A. A general method to coat colloidal particles with titania. *Langmuir* 2010, 26, 9297–9303.

[40] Monfort, O.; Rochb, T.; Satrapinskyy, L.; Gregor, M.; Plecenik, T.; Plecenik, A.; Plesch, G. Reduction of V_2O_5 thin films deposited by aqueous sol–gel method toVO_2(B) and investigation of its photocatalytic activity. *Appl. Surf. Sci.* 2014, 322, 21–27.

[41] Zhang, Z. T.; Gao, Y. F.; Chen, Z.; Du, J.; Cao, C. X.; Kang, L. T.; Luo, H. J. Thermochromic VO_2 thin films: Solution-based processing, improved optical properties, and lowered phase transformation temperature. *Langmuir* 2010, 26, 10738–10744.

[42] Chen, Z.; Gao, Y.; Kang, L.; Cao, C.; Chen S.; Luo, H. Fine crystalline VO_2 nanoparticles: Synthesis, abnormal phase transition temperatures and excellent optical properties of a derived VO_2. *J. Mater. Chem. A* 2014, 2, 2718–2727.

[43] Xu, G.; Jin, P.; Tazawa, M.; Yoshimura, K. Optimization of antireflection coating for VO_2-based energy efficient window. *Sol. Energy Mater. Sol. Cells* 2004, 83, 29–37.

Figure Captions

Figure 1: (a) Wide-range-survey XPS spectra of TiNP@WVNC films on AOP-treated glass slides. (b–d) High-resolution XPS profiles of the (b, c) V 2p core level spectra of the (b) vanadium sol and (c) the TV3 film and (d) Ti 2p and (d) W 4f core level spectra of the TV3 film.

Figure 2: XRD patterns for the pure TiNP, TV1, TV2, TV3, TV4, and pure WVNC films. Diamonds and circles in the XRD patterns mark the main peaks of the M-phase VO_2 and rutile TiO_2, respectively.

Figure 3: DSC curves of WVNCs in the (a) absence and (b) presence of TiNP seeds (Ti/V molar ratio: 0.32).

Figure 4: Top-view SEM images of TiNPs coated with (a) 1, (b) 2, (c) 3, and (d) 4 at. % of the vanadium sol, without sintering.

Figure 5: Top-view SEM images of the TiNP@WVNC films TV1, TV2, TV3, and TV4.

Figure 6: (a) TEM and (b) HRTEM images of a TiNP@WVNC film prepared at a Ti/V molar ratio of 0.32.

Figure 7: (b) SWCAs and roll-off angles of pure TiNP, TV1, TV2, TV3, and TV4 surfaces. (b) SWCAs and (c) roll-off angles of pure TiNP, TV1, TV2, TV3 and TV4 surfaces, plotted with respect to the UV irradiation time. (d, e)

Real-time photographs of water droplets impacting (d) pure TiNP and (e) TV3 surfaces inclined at an angle of 35°.

Figure 8: (a) Transmittance spectra of the TiNP@WVNCs of TV3 at a thickness of approximately 87 nm. Solid and dashed lines represent spectra measured at 50 and 20 °C, respectively.

Table 1 Influence of TiNP seeds on the thermochromic and photocatalytic properties.

Sample	Ti/V[a] (atom %)	Ti/V[b] (atom %)	T_p[c] (°C)	ΔT_H[d] (°C)	Roughness[e] (nm)	$T_{int,20}$[f] (%)	$T_{int,50}$[g] (%)	E_s[h] (%)	K[i]
TV1	1.61	1.54	43.1	5.6	279	43.3	37.5	13.4	0.0013
TV2	0.83	0.89	37.8	4.8	308	49.5	39.7	19.8	0.0015
TV3	0.32	0.39	31.4	3.4	632	56.4	39.3	30.3	0.0017
TV4	0.25	0.28	29.8	2.7	643	58.3	40.1	31.2	0.0018

[a,b]Obtained from XPS and EDX data, respectively; [c]obtained from DSC data; [d]hysteresis between the heating and cooling cycles; [e]obtained from AFM images; [f,g]calcuated by eqn. (1) from 700 to 2500 nm at 20 and 50 °C, respectively; [h]change in values of T_{int} at 20 and 50 °C; [i]rate of MB degradation at 664 nm, determined from UV spectra.

Figure 1

(a)

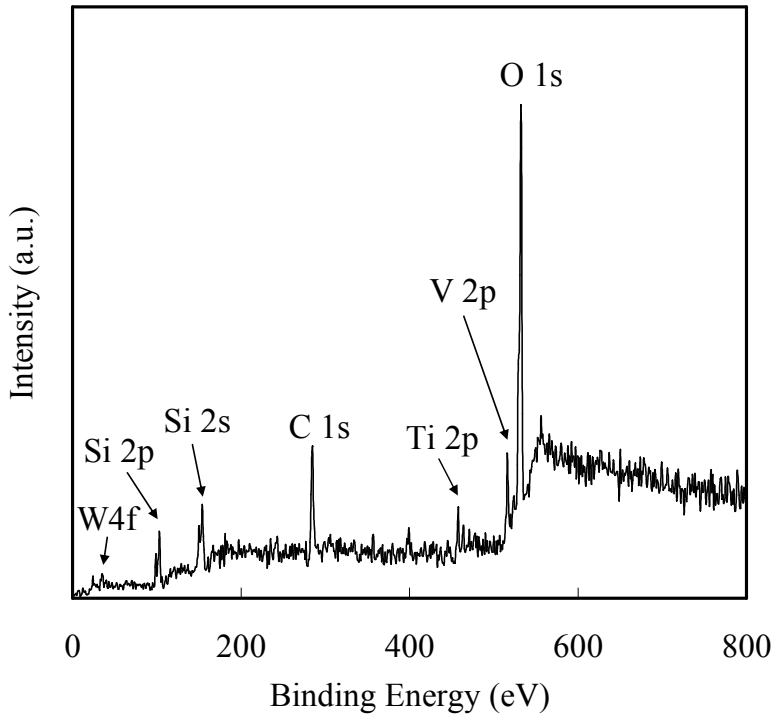

(b)

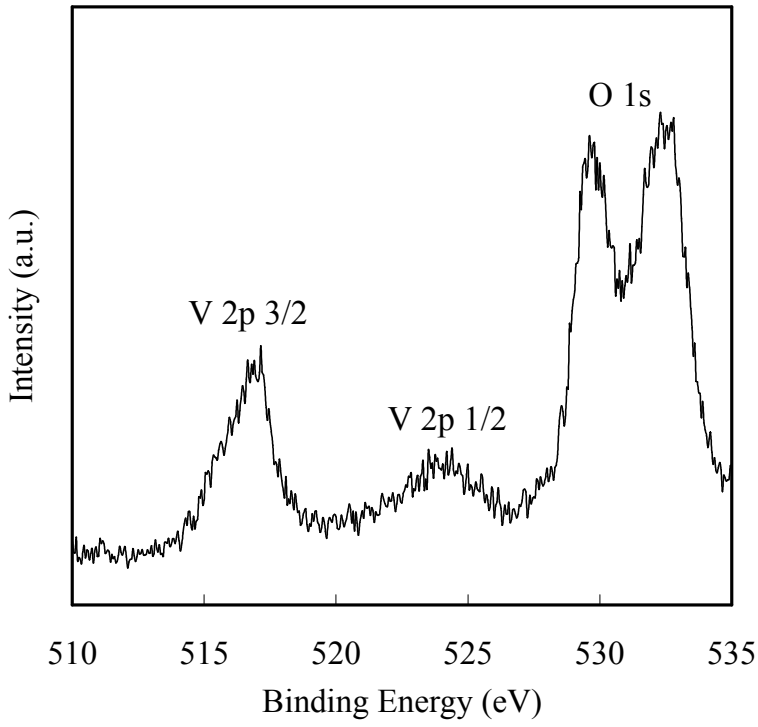

(c)

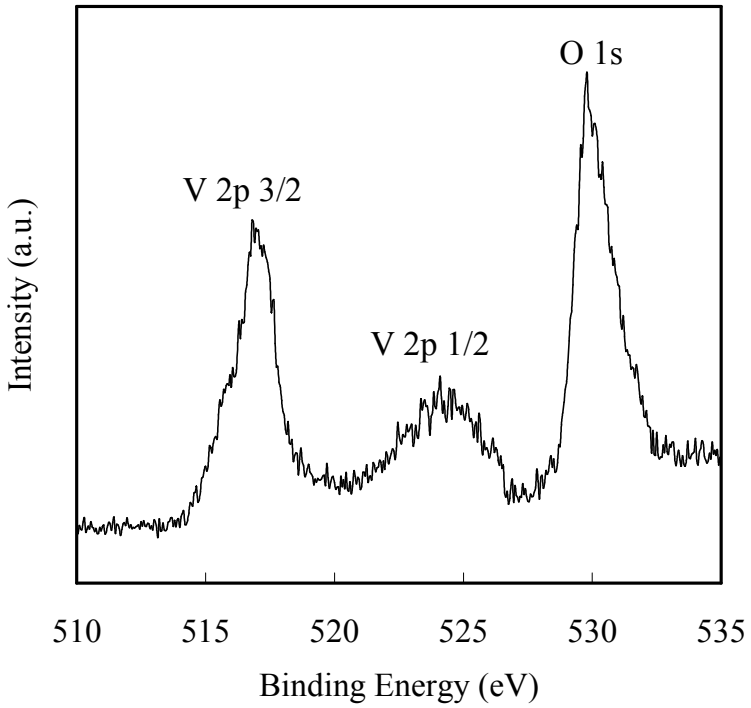

(d)

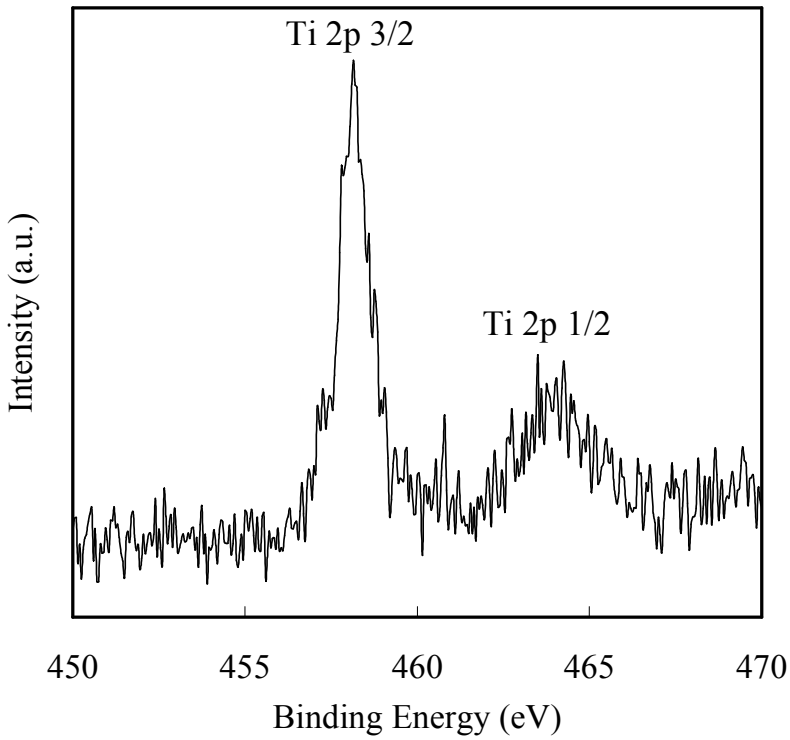

(e)

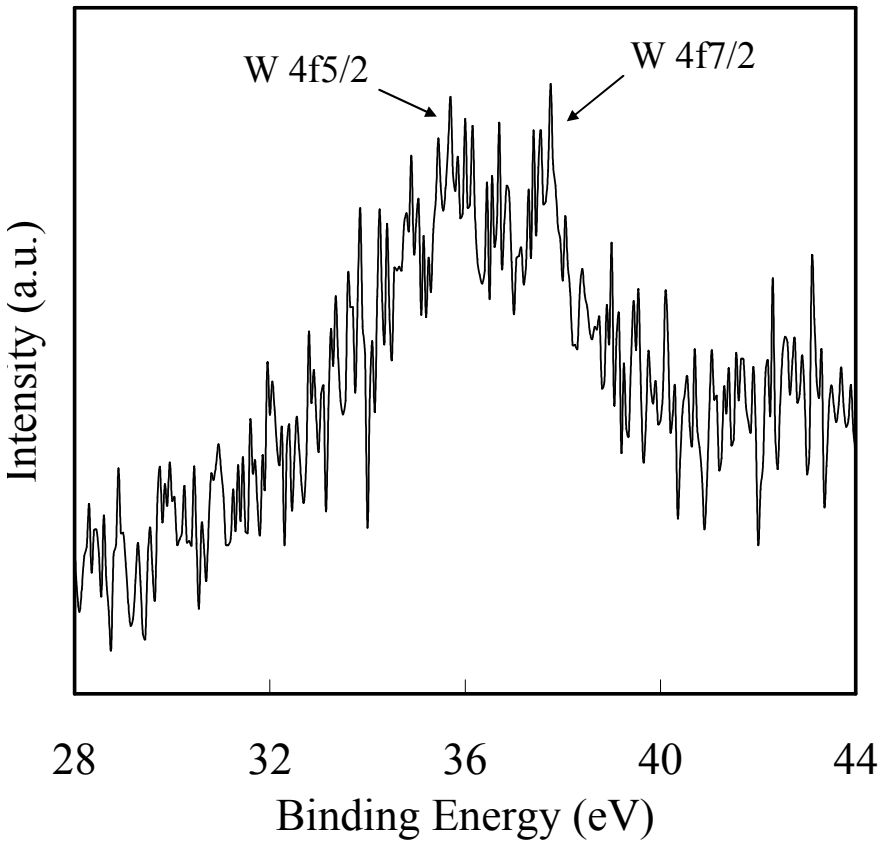

Figure 2

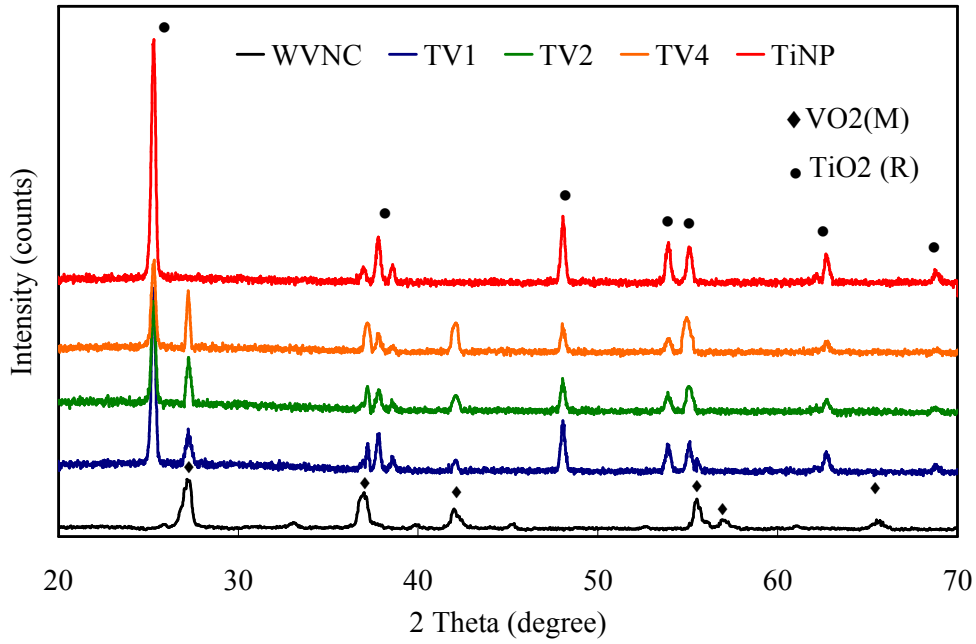

Figure 3

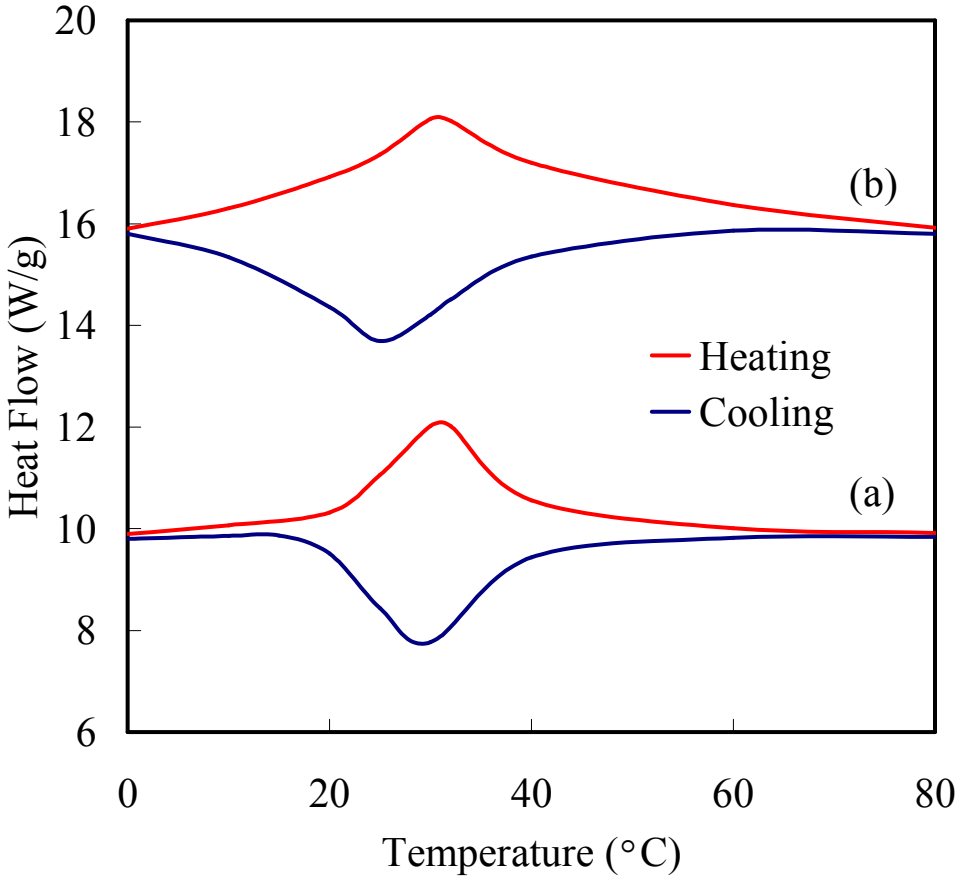

Figure 4

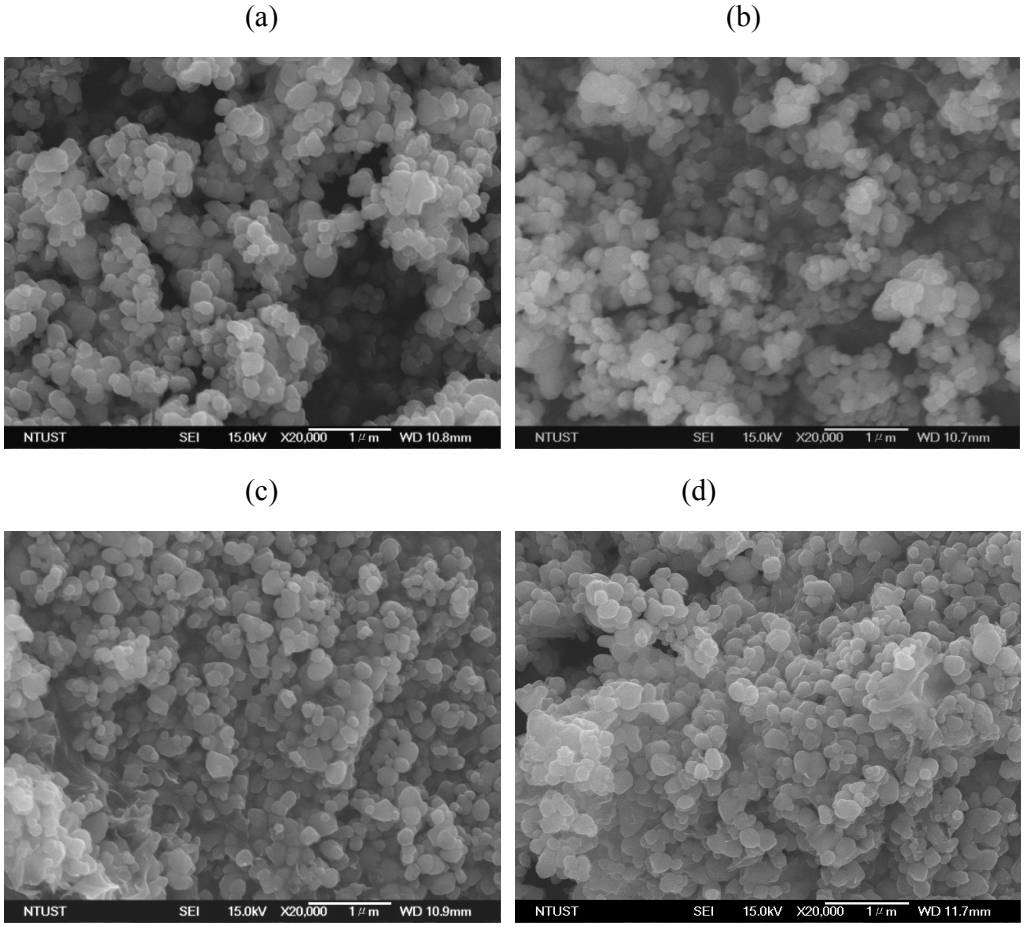

Figure 5

(a)

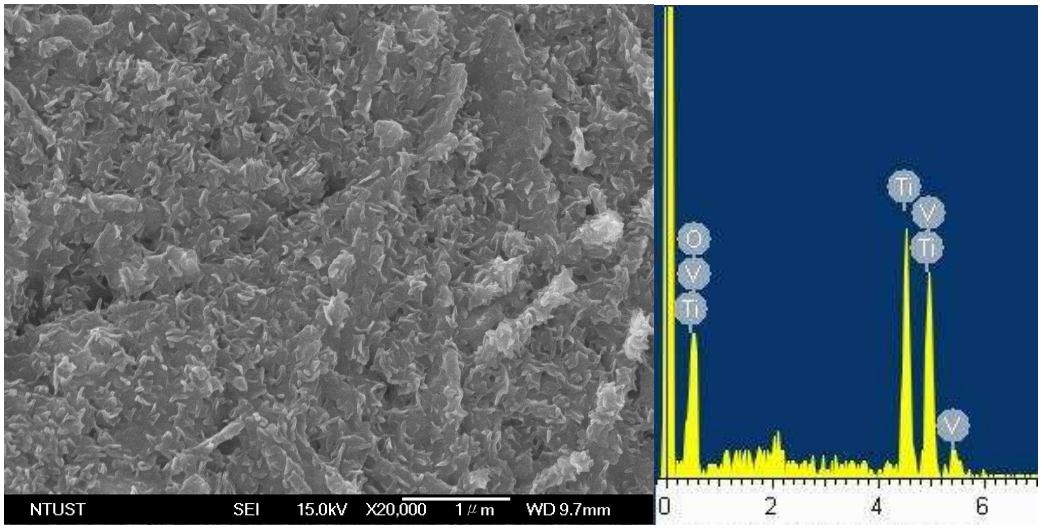

(b)

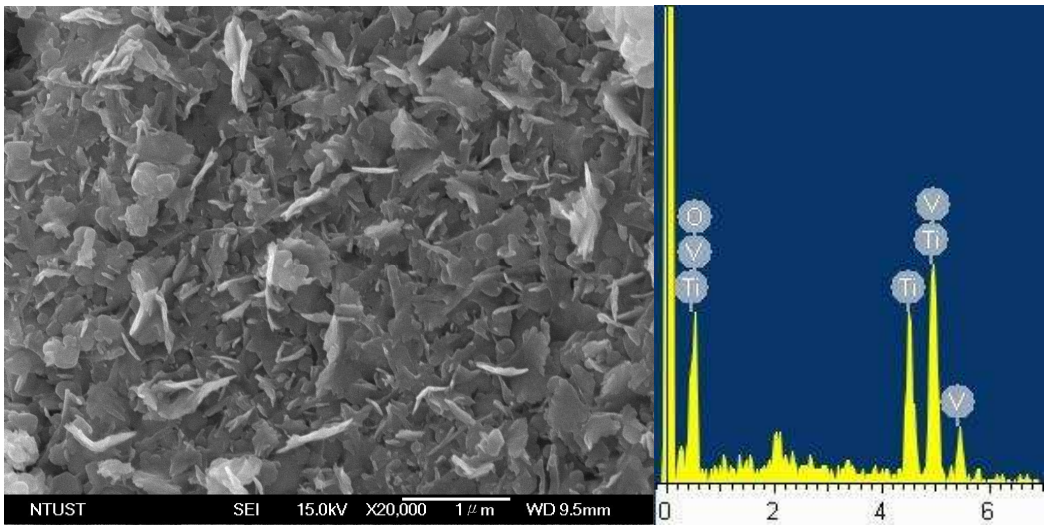

(c)

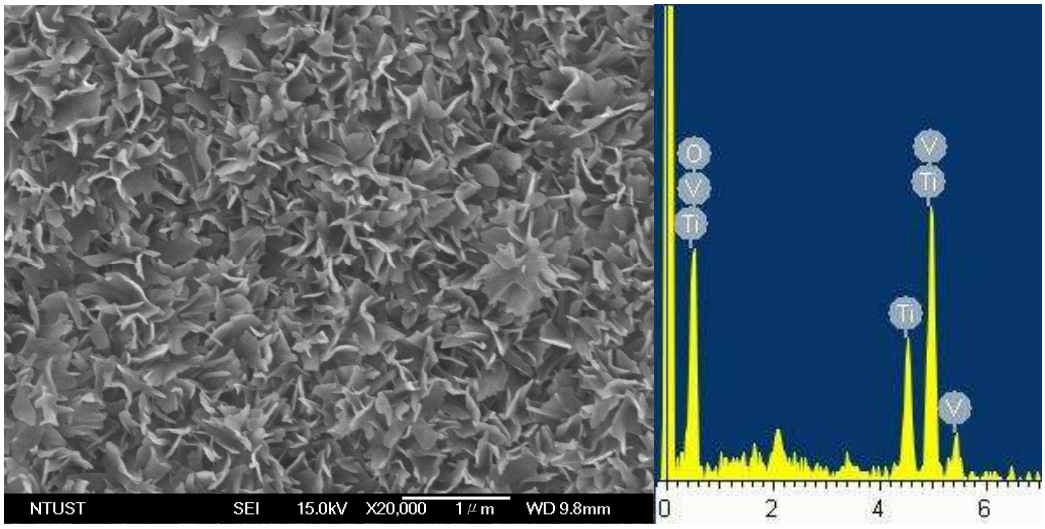

(d)

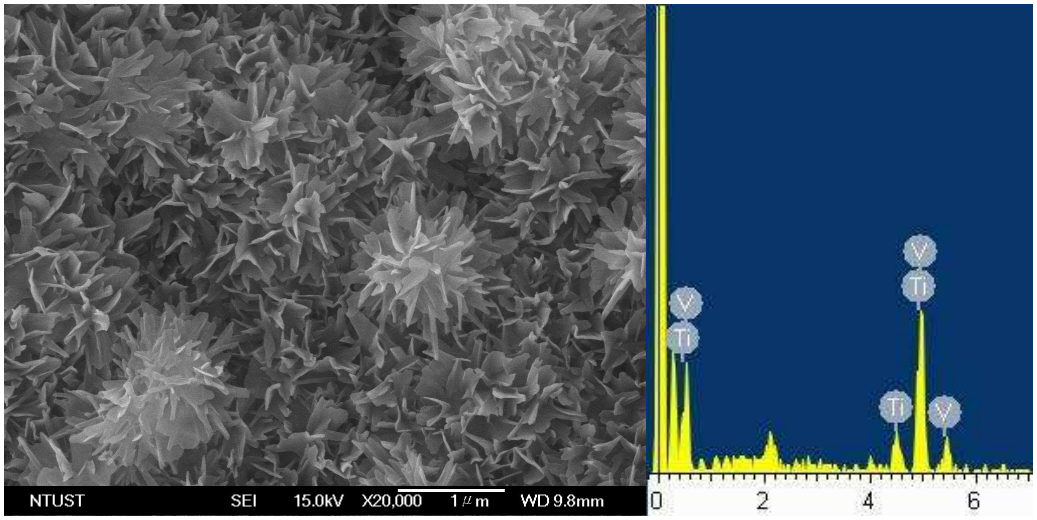

Figure 6

(a)

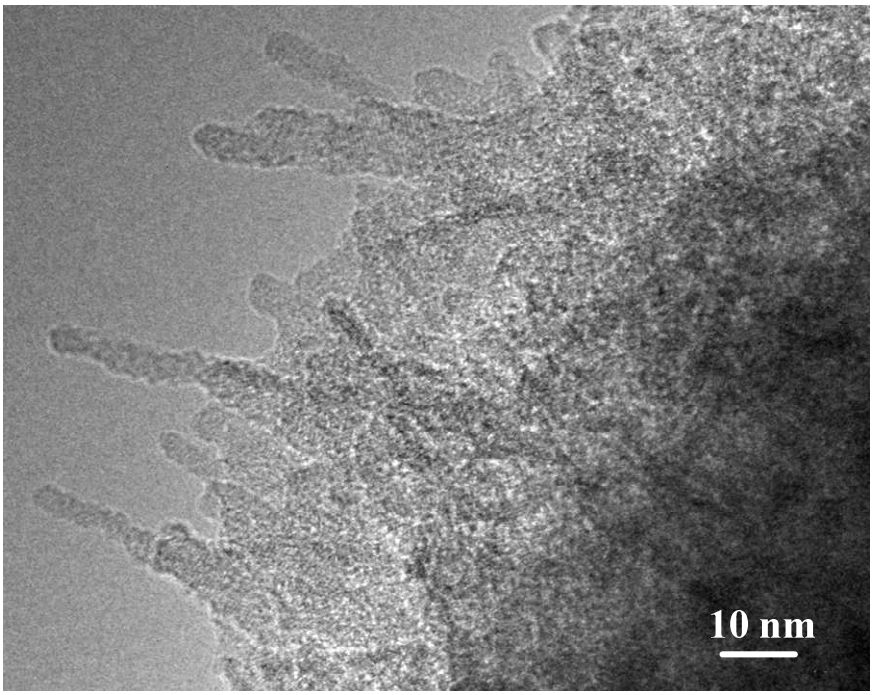

(b)

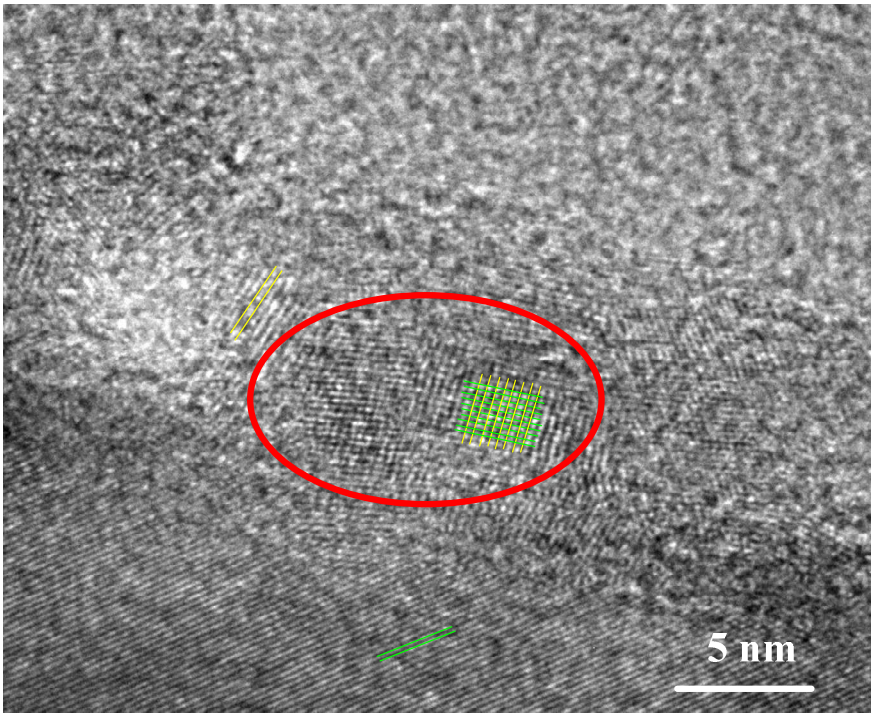

Figure 7

(a)

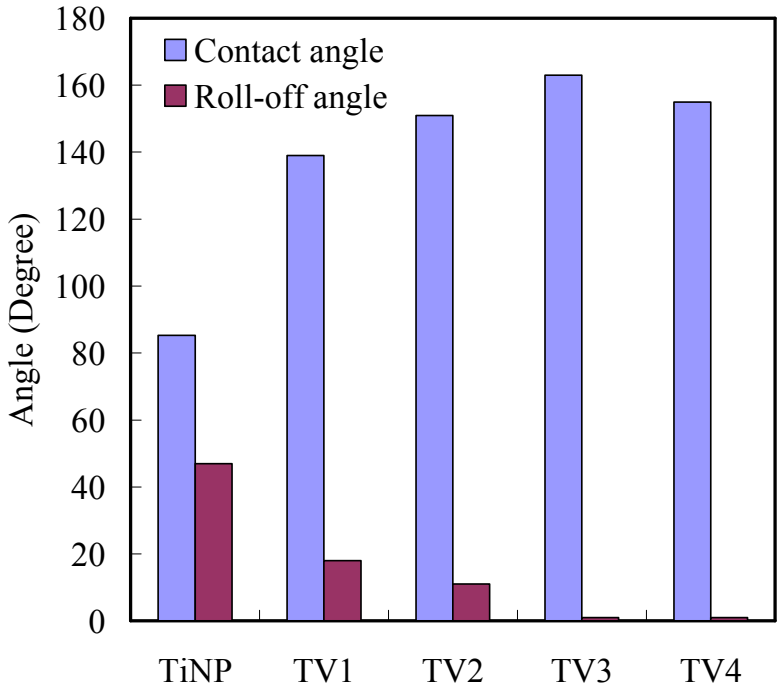

(b)

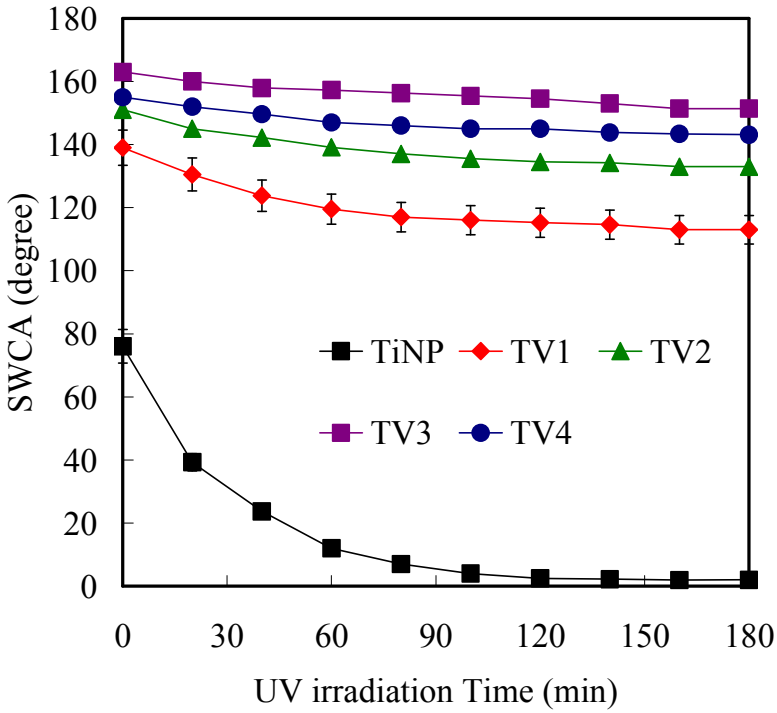

(c)

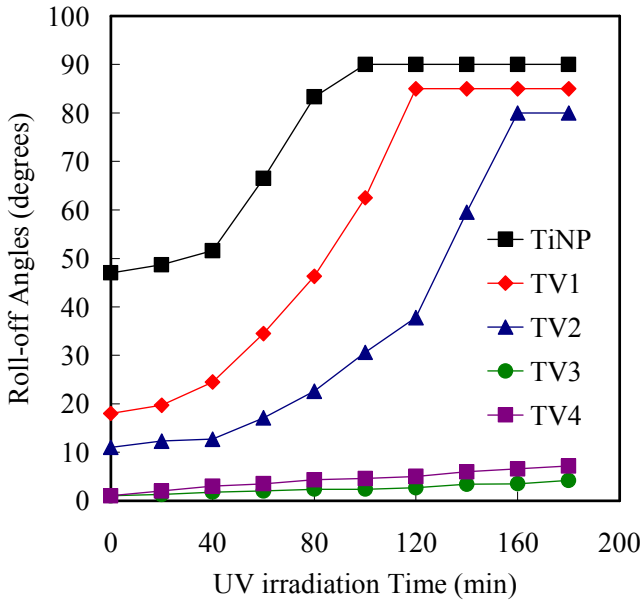

(d)

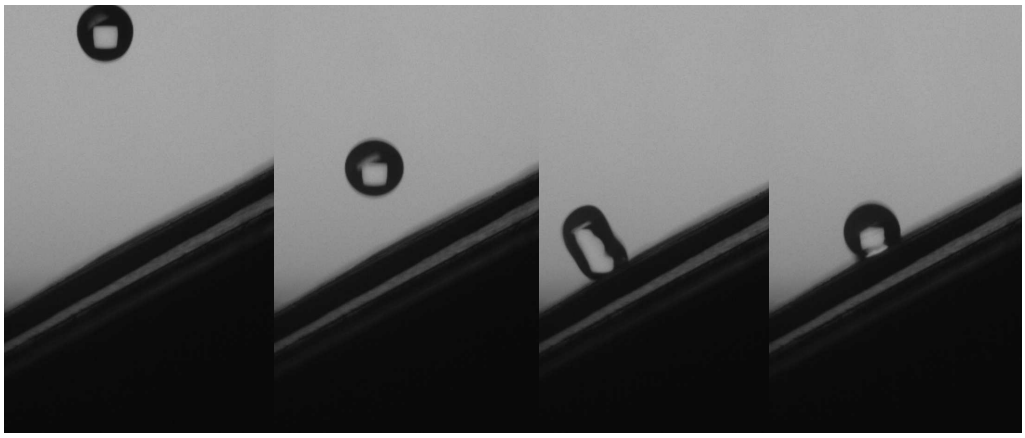

(e)

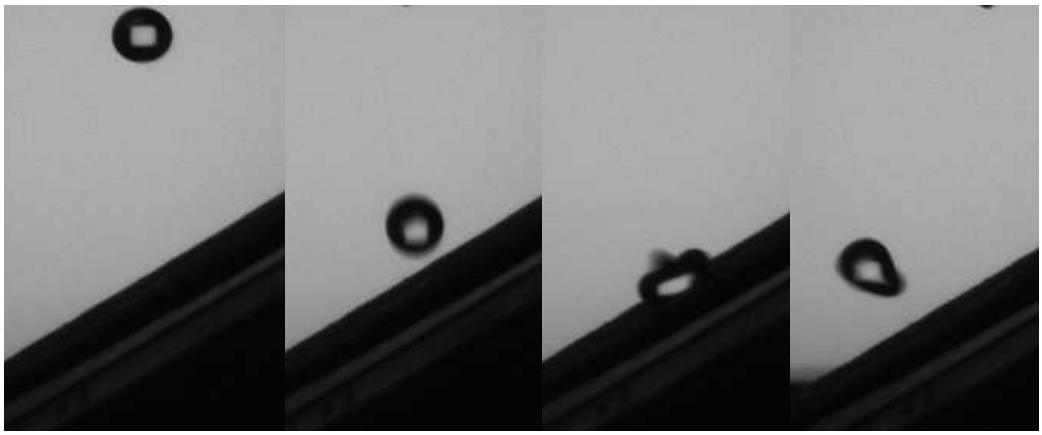

Figure 8

(a)

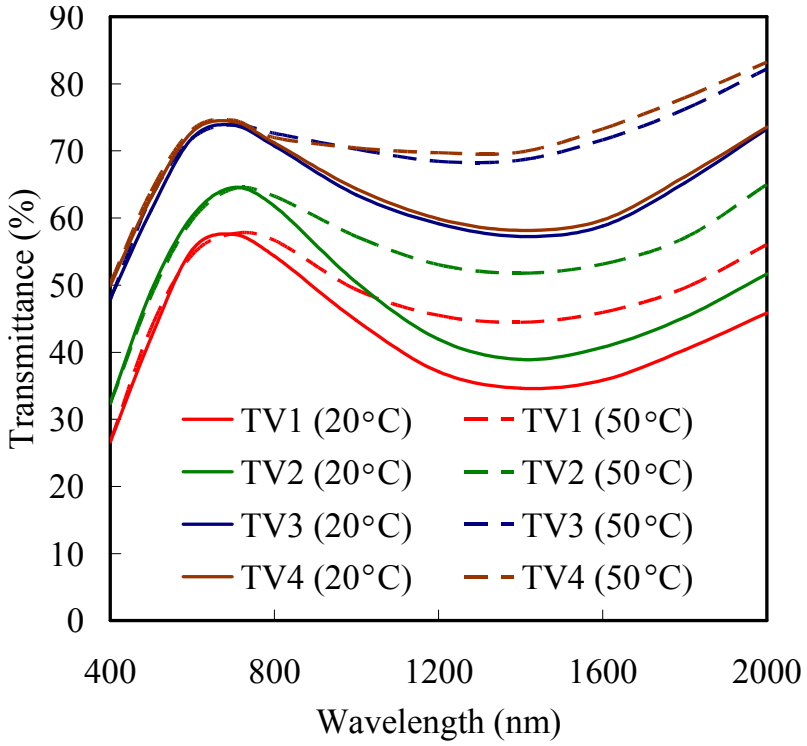

(b)

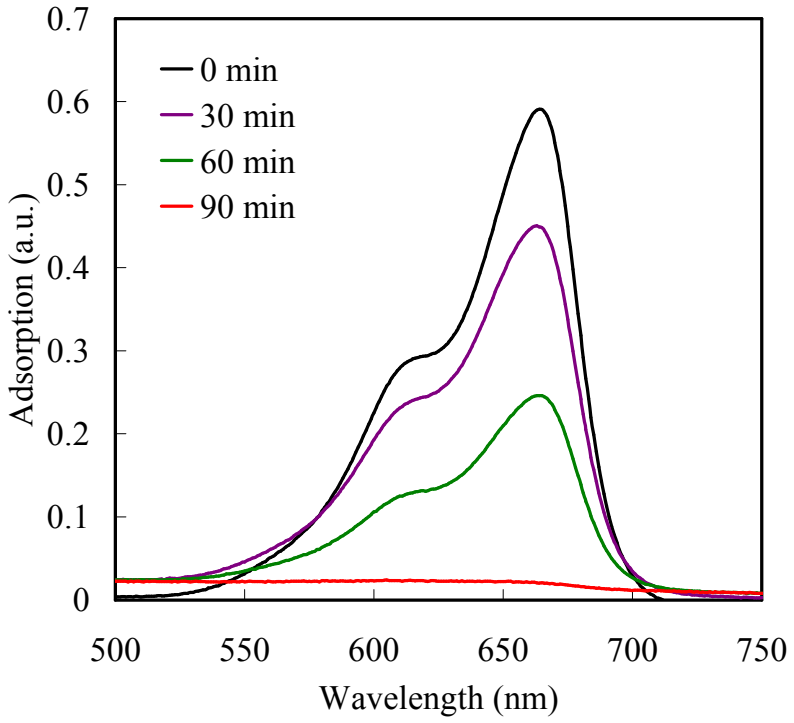

Graphical Abstract

We employed rutile TiO2 nanoparticles (TiNPs) as cores for coating with vanadium sols of various concentrations and a tungsten doping of 2 at%. We grew the W-doped VO2(M) nanocrystals (WVNCs) heteroepitaxially as shells onto the TiNP cores after a sintering process. Needle-like structures gradually appeared for the WVNCs on the TiNP surfaces upon increasing the concentration of the vanadium sol coating. These needle-like structures decreased the surface contact area sufficiently to result in superhydrophobicity. The WVNC shells grew epitaxially on the TiNP seeds and enhanced the visible transmittance and near-infrared switching efficiency, due to the needle-like structures, similar to the behavior of an antireflection coating.